2014

Large wind turbine structural load control: trailing edge deformation mechanism for active variable-camber blade

Michael Dicker
University of Wollongong, mpd334@uowmail.edu.au

Buyung Kosasih
University of Wollongong, buyung@uow.edu.au

Publication Details

Dicker, M. & Kosasih, B. (2014). Large wind turbine structural load control: trailing edge deformation mechanism for active variable-camber blade. Wind Engineering, 38 (4), 425-440.

Large wind turbine structural load control: trailing edge deformation mechanism for active variable-camber blade

Abstract
Blade root fatigue stress, primarily resulting from wind shear and turbulence, is a critical factor in wind turbine design. Blade mounted aerodynamic control devices have been shown to have the potential to reduce this. However, limited research exists into suitable devices. The blade designed in this work addresses this by employing an actuated compliant mechanism, contained within a flexible matrix composite structure. The resulting mechanism design achieves a sectional change in lift coefficient of ΔCL + 0.4 to -0.15. The performance of the blade is analysed with a quasi-steady time marching BEM model. A reduction of 21.59% in the standard deviation of the flap-wise bending moment comparable to previous load control investigations has been achieved.

Keywords
airfoil, compliant mechanism, load control, variable-camber, wind turbine

Publication Details
Dicker, M. & Kosasih, B. (2014). Large wind turbine structural load control: trailing edge deformation mechanism for active variable-camber blade. Wind Engineering, 38 (4), 425-440.

Large Wind Turbine Structural Load Control: Trailing Edge Deformation Mechanism for Active Variable-Camber Blade

Michael Dicker[a] and Buyung Kosasih[b]
School of Mechanical, Materials and Mechatronics Engineering, University of Wollongong, NSW 2500 Australia.
[a]mpd334@uowmail.edu.au, [b]buyung@uow.edu.au

Received 8/2/2013; Revised 4/10/2014; Accepted 4/28/2014

ABSTRACT

Blade root fatigue stress, primarily resulting from wind shear and turbulence, is a critical factor in wind turbine design. Blade mounted aerodynamic control devices have been shown to have the potential to reduce this. However, limited research exists into suitable devices. The blade designed in this work addresses this by employing an actuated compliant mechanism, contained within a flexible matrix composite structure. The resulting mechanism design achieves a sectional change in lift coefficient of ΔC_l + 0.4 to −0.15. The performance of the blade is analysed with a quasi-steady time marching BEM model. A reduction of 21.59% in the standard deviation of the flap-wise bending moment comparable to previous load control investigations has been achieved.

Keywords: airfoil, compliant mechanism, load control, variable-camber, wind turbine

1. INTRODUCTION

Efficient and robust structural load control is crucial for continued development of ever larger wind turbines (Barlas and van Kuik, 2009) with blade root fatigue stress being a critical factor in large wind turbine design (Veers et al., 2003). These fatigue loads are the result of aerodynamic effects such as wind shear, gusts, tower shadow, turbulence, and yaw misalignment. As the size of turbine blades increase, aerodynamic loads also increase due to the greater leverage now exerted by tip loading and the exposure of the swept area of the blades to greater spatial discrepancies in the wind field (both shear and stochastic disturbances).

One promising way to reduce loading is through the integration of distributed aerodynamic controls and sensors within the blades often referred to as ‘smart rotor control’. The core idea behind this is that the local aerodynamic performance of a section of blade can be adjusted to cancel out the fluctuating loads. For example, this may mean reducing the local lift coefficient of blade sections as they pass through the top of the rotation cycle. This can cancel out the increased aerodynamic loading from wind shear. Sensors would be distributed along the blade allowing individual sections of the blade to react to highly localized disturbances periodically sampled as the blade rotates, having a major contribution to fatigue loading.

Significant research in the field has already been conducted (Barlas and van Kuik, 2010). The 2010 review concluded that the potential for load reduction from applied aerodynamic control was now proven. However, great challenges still exist in moving from research to production. The most critical challenge was noted as the need to develop a scalable smart rotor design that can meet the requirements for load control, without compromising the current reliability and safety standards of wind turbine blades.

Recently Lackner and Kuik (2011) investigated the application of actively controlled trailing edge flaps as smart rotor control devices where trailing edge flaps are added between 70 to 90%

span. The load reduction potential compared favourably with pitch control approach. This paper aims to facilitate alternative development of a wind turbine blade design capable of providing active structural load control by deformation mechanism based variable-camber wind turbine blade. The proposed mechanism involves less moving part hence should have higher life cycle capacity. Design methodology is presented, before the theoretical blade performance is quantified.

2. METHOD AND DESIGN DEVELOPMENT

The methodology consisted of four main parts. Firstly, key design attributes relating to both turbine operation and load control were selected. Then these attributes were used to guide the design of the variable-camber mechanism. The performance of the variable camber mechanism was then quantified. Finally, this performance data was used as an input to determine the overall load control potential of the design.

2.1. Selection of key design attributes

Reference turbine. NREL/UpWind 5 MW offshore wind turbine was chosen as the reference turbine in this study (Musial et al., 2009). The NREL/UpWind 5MW offshore wind turbine blade uses single airfoil profile (NACA-64618) for the outer 30% of the blade. As one would expect, the higher relative velocity effect leads to devices placed at the tip of the blade having a greater effect than devices placed at the blade root. Limiting active load control to the outer span of the blade achieves a compromise between desired load alleviation, and cost, weight, and power consumption factors. In this work variable-camber mechanism is applied in the 30% span.

Change in lift coefficient. Lackner and Barlas (2008) identified that for the NREL/UpWind 5 MW offshore wind turbine to achieve theoretically required change in lift coefficients, control of all fluctuations in aerodynamic load must be applied between 70 to 90% of blade span. Investigation by Marrant and van Holten (2006) concluded that for 30% smart structure length, variable-camber/flap active control with static $\square C_L \pm 0.4$ was twice as effective as MEM-tab control with static $\square C_L \pm 0.3$ at reducing load fluctuations, despite having reduced bandwidth. Obviously there is a rather complicated relationship between bandwidth and lift coefficients, and the eventual performance will depend upon a myriad of additional factors. However, it seemed reasonable to the authors that the design factors imposed by Marrant and van Holten of static $\square C_L \pm 0.4$ was an excellent value for the preliminary design to aim towards.

Bandwidth. From power spectral density (PSD) data, Barlas and van Kuik (2010) concluded that the load spectrum with significant energy was in the 0–6 Hz range. As such, to fully eliminate the load fluctuation in this range, the actuator bandwidth should be twice that of the disturbance namely 12 Hz.

Trailing edge deflection. The desired profile deviation required to achieve the goal of $\square C_L \pm 0.4$ for the NACA 64618 airfoil was then determined. To do this a program called XFLR5 was used to generate aerodynamic data on a number of modified NACA 64618 profiles. XFLR5 is the latest version of the well known XFOIL developed by Drela (1989).

To generate static $\square C_L \pm 0.4$, an approximate TE deflection of +1.8% chord (up) to −2.76% chord (down) was found to be required (see Figure 1). This would mean that for the largest section of the active control part of the blade, with the chord length of approximately 3000 mm, the TE deflection required is −83 mm to +54 mm.

Operating life. Another key design attribute that was quantified before the design commenced was the operating life, and maintenance restrictions applied to the blade. Commercial blades have

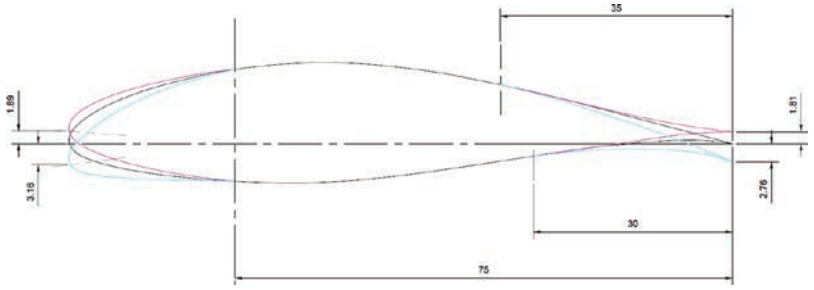

Figure 1. The required profile deformation (in % chord units) to achieve $\Delta C_L \pm 0.4$

economic lives of 20 to 30 years, over which time they will experience up to 10^9 stress cycles (Veers et al., 2003). Maintenance of any control devices on, or particularly in the blade would be near impossible. If the technology was to be applied to an ultra-large offshore generating unit, this type of maintenance would be extremely expensive, and would present significant safety risks. As such, the actuator and variable camber mechanism must have comparable economic life, cycle capacity, and limited maintenance requirements for the solution to be deemed viable and beneficial.

The key design attributes of the TE deformation mechanism can be summarised as follow

- The design is based on the NREL/UpWind 5MW reference turbine.
- The active variable-camber control to be applied to the outer 30% of the blade, allowing the variable camber mechanism to be applied to a single airfoil profile, the NACA 64618.
- The mechanism is capable of generating a change in lift coefficient of $\Box C_L \pm 0.4$.
- The mechanism has a bandwidth of 12 Hz.
- The smoothly deformable section profile achieves a TE deflection of +1.8% chord (up) to –2.75% chord (down).
- The system is capable of a near maintenance free operating life of 20–30 years, consisting of up to 10^9 cycles.

2.2. Development of the variable-camber mechanism

Selection of camber mechanism. Many mechanisms have been developed for displacement multiplication of piezoelectric actuators (Jensen et al., 2007). Many of these were developed for active vibration control in helicopter rotor blades. However, there are some differences that need to be considered, namely in regards to scalability, and maintenance/cycle life considerations. When these factors are considered, so called compliant mechanism become the most promising solution. Compliant mechanisms are those which transmit force/motion through elastic deformation of the mechanism members. They have no conventional hinge joints, and as a result these mechanisms generally exhibit the benefits of reduced complexity, high accuracy, and zero wear and backlash, while allowing for simple, and scalable integration with actuators (Kota et al., 2003).

Many configurations and optimisation strategies have been developed for airfoil morphing compliant mechanisms (Baker and Friswell, 2009; Gupta et al., 2010). These strategies generally aim to maximize the actuated TE tip deflection to air load deflection ratio (within acceptable limits), by changing the placement and size of actuation and static members within a determinate truss-like structure mounted inside the airfoil. The relatively simple mechanism configuration is chosen as shown in Figure 2 (Gandhi et al., 2008).

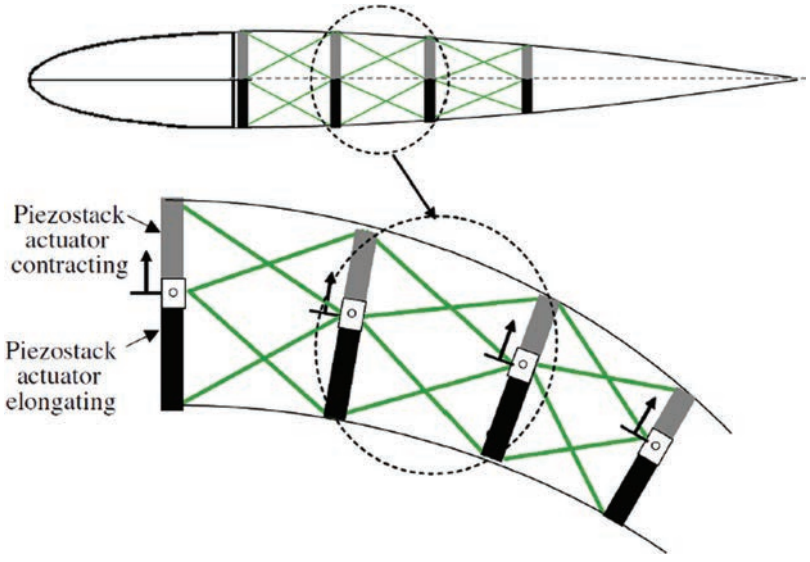

Figure 2. The variable camber compliant mechanism developed by Gandi et al. (2008) for use in helicopter rotor blades, the vertical members are the actuators, while the cross members are the static members; expansion of the lower actuators and corresponding contraction of the upper members leads to camber gain

Development of variable-camber compliant mechanism. Information on the number and spacing of actuators required in order for adequate profile deviation must be determined. One simple way of approximating this was with kinematic analysis, whereby the flexible joints were treated as pins and the cross members as fully rigid members. The mechanism can be analysed as follows, whereby three sets of non-linear simultaneous equations can be formed using the known values of actuator and cross-member length (see Figure 3(a)), as well as the fixed coordinates of the top and bottom of the first actuator stack.

$$\left(M_{2,x} - U_{1,x}\right)^2 + \left(M_{2,y} - U_{1,y}\right)^2 = A^2 \tag{1}$$

$$\left(M_{2,x} - L_{1,x}\right)^2 + \left(M_{2,y} - L_{1,y}\right)^2 = D^2 \tag{2}$$

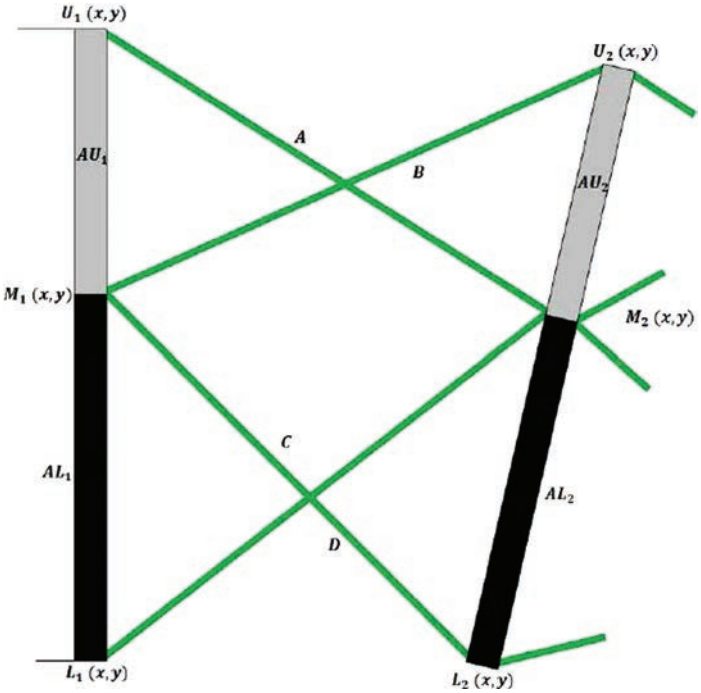

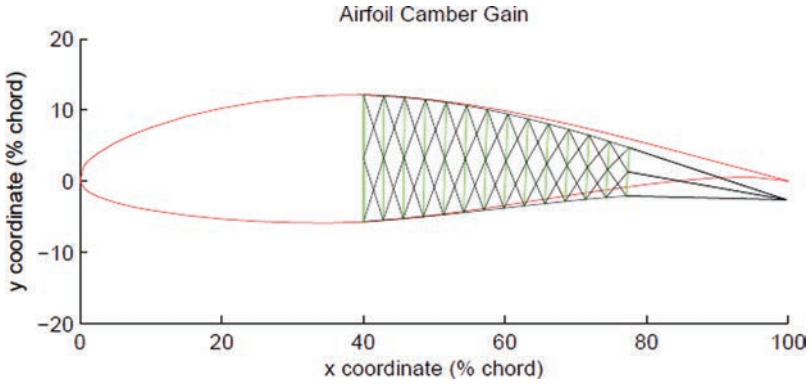

Figure 3. (a) One element of the compliant mechanism is shown; the nomenclature used in the following kinematic analysis is displayed (b) Airfoil with 14 actuator stacks spaced at 2.88% chord intervals starting at the 40% chord, a negative TE deflection of 2.62% chord is observed

These are solved to find $M_2\,(x, y)$.

$$\left(U_{2,x} - M_{2,x}\right)^2 + \left(U_{2,y} - M_{2,y}\right)^2 = AU_2^2 \tag{3}$$

$$\left(U_{2,x} - M_{1,x}\right)^2 + \left(U_{2,y} - M_{1,y}\right)^2 = B^2 \tag{4}$$

These are solved to find $U_2\,(x, y)$.

$$\left(L_{2,x} - M_{2,x}\right)^2 + \left(L_{2,y} - M_{2,y}\right)^2 = AL_2^2 \tag{5}$$

$$\left(L_{2,x} - M_{1,x}\right)^2 + \left(L_{2,y} - M_{1,y}\right)^2 = C^2 \tag{6}$$

These are solved to find $L_2\,(x, y)$. This method can be followed through the mechanism, eventually revealing TE displacement. An example of airfoil TE deflection of 14 actuator stacks mechanism is shown in Figure 3(b).

FE analysis of variable-camber performance capabilities. Based on the kinematic analysis, FE analysis of a section of the variable-camber blade is performed. The analysis was performed using the software package FEMAP with NX Nastran solver. The model used in the analysis is a 3000 mm chord length section, with a depth of 200 mm. This represents a section of the blade where variable camber mechanism starts at radius of approximately 44 m and where the span between piezoceramic stack supports is the greatest hence location of worst case loading of the flexible skin. The initial geometry was established from the minimum-camber kinematic result, in order to allow the FEA model to actuate in one direction only. The model employs FEMAP plate and laminate elements. These are 2D elements, which allow for excellent modelling of thin, plate-like members in the model, without having to use an excessive number of elements as would be required if modelling with 3D elements.

The model was fixed by the blade surface in front of the variable-camber mechanism, whilst a worst case pressure map was applied to the surface behind this point, extending over the variable-camber mechanism to the trailing edge. The piezoceramic stack actuators were modelled as non-linear spring elements (governed by a step function), with actuation forces applied at their ends, such that they are placed in tension. These non-linear springs exhibit zero spring stiffness up to the allowable piezoceramic deformation (0.15%), then the element stiffness becomes near infinite, preventing further extension. This representation of the actuators is deemed accurate for this preliminary analysis.

The main philosophy employed in sizing of the compliant mechanism members was to gain maximum camber change (measured by TE deflection), whilst ensuring the stress in the compliant mechanism remained below the material fatigue limit. The compliant mechanism is designed out of the engineering polymer Delrin, which has a fatigue limit in the 20 MPa to 30 MPa range (Delrin, 2011).

Figure 4 shows three outputs of the non-linear routine for 10%, 50% and 100% load progressions. The contour plot displays the von Mises stress in the top and bottom surface of the plate elements, and the major principal stress in the first ply of the flexible skin laminate. The ultimate trailing edge deflection was found to be 124 mm, which is a percent chord value of 4.13%.

2.3. Aerodynamic performance

The developed variable-camber mechanism was then implemented in finite element model described above to capture the range of profile change achievable from the final device. Resulting profile changes were then fed back into XFLR5 to determine the available change in aerodynamic performance from the device. In Figure 5 it can be seen that the resulting change in lift coefficient in the linear range of the plot is around $C_L + 0.4$ to -0.15. All the lift data for all outputs is plotted as a 3D mesh (Figure 5). This displays a surface plot of lift coefficients as a function of angle of attack and TE deflection.

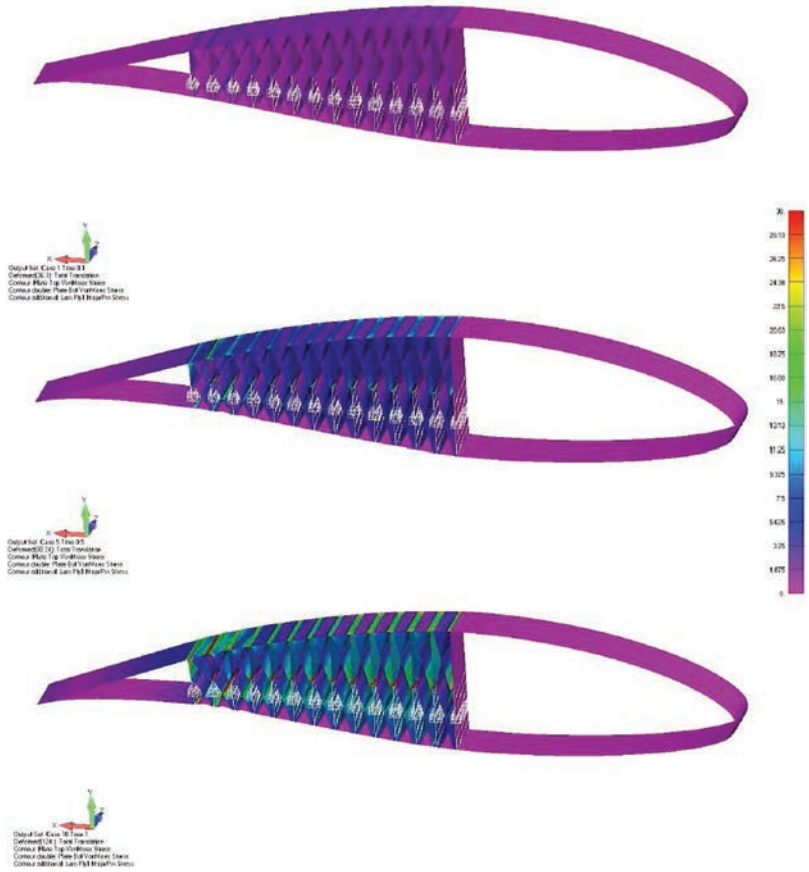

Figure 4. Three outputs of the non-linear routine for 10%, 50% and 100% load progressions, displaying the von Mises stress in the top and bottom surface of the plate elements, and the major principal stress in the first ply of the flexible skin laminate

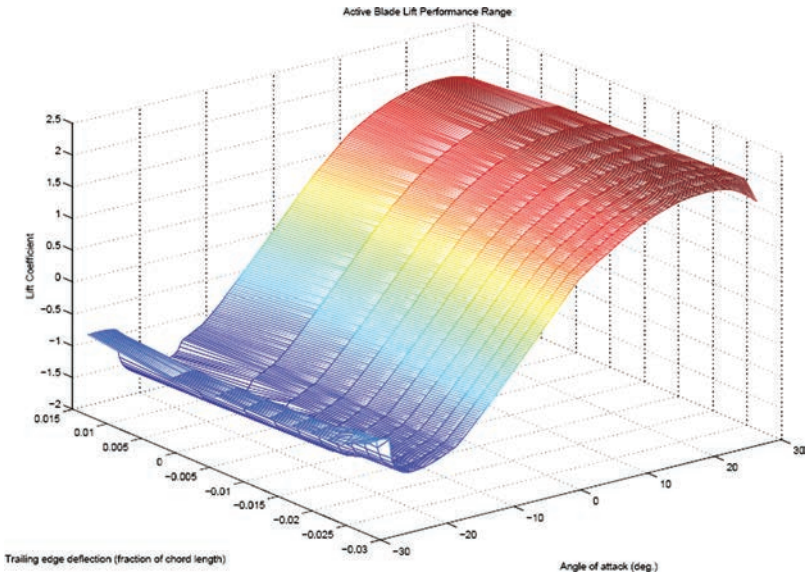

Figure 5. The coefficient of lift and angle of attack plot extended for all camber positions

3. BLADE AERODYNAMIC AND STRUCTURAL ANALYSIS

In this section, the performance of the variable-camber blade is assessed. Firstly, a wind field must be developed, whereby time series data for wind speed at a number of spatial points within the sweep of the rotor are generated. The wind speed data is fed into a Blade Element Momentum (BEM) program to determine the aerodynamic loads on the blade. Also inputted into the BEM program are the variable section lift coefficients, determined in the previous section. Finally the structural component is implemented whereby the blade root stress is calculated from the aerodynamic load output of the BEM program and the weight effects.

3.1. Wind field synthesis

In order for this analysis to be both representative of real world conditions, and comparable to other research, a characteristic wind field must be synthesised. Guidelines for characteristic wind conditions are outlined in the European standards for Wind Turbine Design Requirements BS EN 61400-1:2005. The standard presents suitable models and values for the turbulence intensity, power spectral densities, and spatial coherence, as well as for wind shear (IEC 61400-1, 2005). In order to get useful information from the frequency-dependent functions of the characteristic wind field, a characteristic series of correlated time series sets of wind data will be required. A number of methods can be used to achieve this; the one used in this work is the Sandia Method, developed by Veers (1988). The method has been discussed in a number of sources, including Winkelaar (1992) and Manwell (2009). Figure 6 shows selected results from the wind field synthesis.

3.2. Blade aerodynamic performance calculation

At the core of most calculations for the aerodynamic performance of wind turbines is blade element momentum theory (BEM). There are three main inputs to the BEM calculation namely: wind field, blade geometry and airfoil data.

Wind field. The first is the wind field generated in accordance with the methods outlined in section 3.1. At each time step, the absolute location of each control point on the blade is determined, relative to the wind field. A typical wind field grid is shown in Figure 7. The local free stream wind velocity U is then calculated using linear interpolation in both time and space (simulation time and wind grid coordinate domains).

Blade geometry. The local chord c, and twist angle θ_T are required for each control point of local radius r, as well as information on the airfoil section. This information is taken from Musial et al. (2009), and presented in Table 1. The overall radius of the blade is 63 m, and denoted by R.

Airfoil data. The lift and drag data for the inner sections of the blade (cylinders and DU foils) are taken from Musial et al. (2009). These have been corrected for rotational stall delay using the Selig and Eggars method, while the drag coefficients are corrected using the Viterna method assuming an aspect ratio of 17. For the active portion of the blade, the lift and drag coefficients are generated for each camber variation of the base NACA 64618 profile using the program XFLR5.

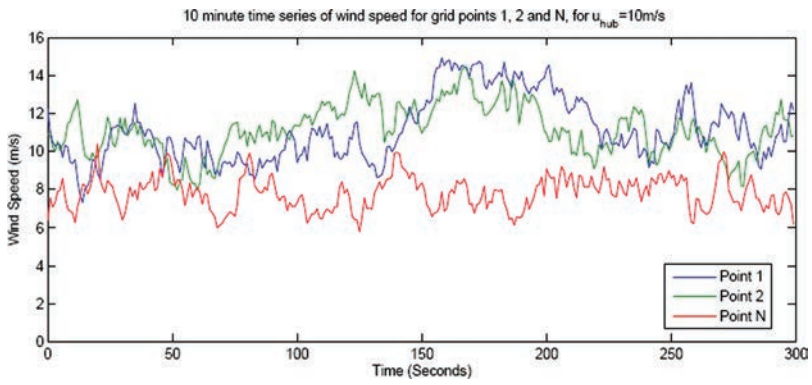

Figure 6. The 10 minute wind speed time series for points 1, 2 and N in the wind field grid, the correlation between points 1 and 2 is evident, whilst the data for point N at the other corner of the field shows reduced correlation with points 1 and 2, and has a mean value significantly less, demonstrating the effect of vertical wind shear

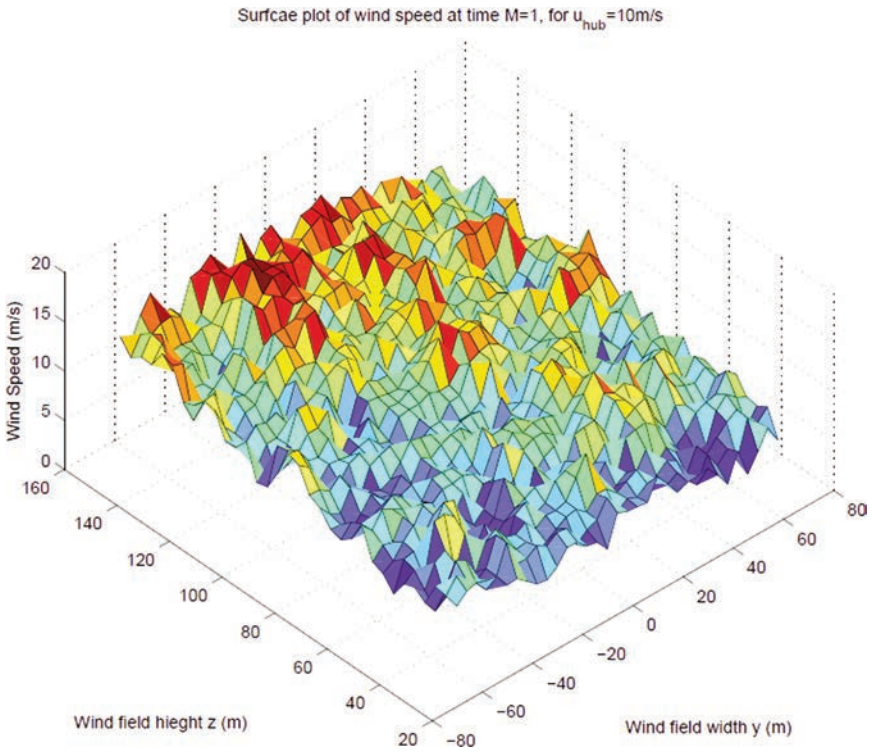

Figure 7. A three dimensional representation of the wind field showing the correlation between closely grouped grid points, and the effects of wind shear on the field

Table 1. Blade data for the NREL 5MW reference turbine

Control Point	Radius (m)	Twist	Δr (m)	Chord (m)	Airfoil
1	1.5	13.308	1.3667	3.542	Cylinder 1
2	2.8667	13.308	2.7333	3.542	Cylinder 1
3	5.6	13.308	2.7333	3.542	Cylinder 1
4	8.3333	13.308	3.4167	4.167	Cylinder 2
5	11.75	13.308	4.1	4.557	DU40
6	15.85	11.48	4.1	4.652	DU35
7	19.95	10.162	4.1	4.458	DU35
8	24.05	9.011	4.1	4.249	DU30
9	28.15	7.795	4.1	4.007	DU25
10	32.25	6.544	4.1	3.748	DU25
11	36.35	5.361	4.1	3.502	DU21
12	40.45	4.188	4.1	3.256	DU21
13	44.55	3.125	4.1	3.01	NACA64618
14	48.65	2.319	4.1	2.764	NACA64618
15	52.75	1.526	3.4167	2.518	NACA64618
16	56.1667	0.863	2.7333	2.313	NACA64618
17	58.9	0.37	2.7333	2.086	NACA64618
18	61.6333	0.106	1.3667	1.419	NACA64618
19	63	0	0	0.5	NACA64618

The lift coefficients were then corrected using the Du-Selig method (Selig and Du, 1998), developed from the stall delay principles analysis given below.

$$C_l = C_{l,2D} + f_l\left[C_{l,slope}\left(\alpha - \alpha_0\right) - C_{l,2D}\right] \tag{7}$$

$$C_d = C_{d,2D} + f_d\left[C_{l,2D} - C_{d,0}\right] \tag{8}$$

and

$$f_l = \frac{1}{2\pi}\left[\frac{1.6c/r\left(1-c/r\right)^{\frac{R}{\Lambda r}}}{0.1267\left(1+c/r\right)^{\frac{R}{\Lambda r}}} - 1\right] \tag{9}$$

$$f_d = \frac{1}{2\pi}\left[\frac{1.6c/r\left(1-c/r\right)^{\frac{R}{2\Lambda r}}}{0.1267\left(1+c/r\right)^{\frac{R}{2\Lambda r}}} - 1\right] \tag{10}$$

$$\Lambda = \frac{\Omega R}{\sqrt{U^2 + \left(\Omega R\right)^2}} \tag{11}$$

where Ω is blade angular velocity, $C_{l,slope}$ is the gradient of the angle of attack with respect to the coefficient of lift curve and is approximately 0.1, and α_0 is the angle of attack for which zero lift is generated.

3.3. Structural calculation

Since for this study we are primarily focused on reduction of blade root stress, caused in large part by the flap-wise bending moment, sectional normal stress need to be calculated by the BEM approach (Manwell, 2009). Based on this approach a time marching aerodynamic load output from the BEM program and weight effects can be calculated.

For the simple comparative results desired for this preliminary design, it is appropriate to treat the blade as a rigid member. The loads considered in this analysis are displayed in Figure 8. The blade root flap-wise bending moment is determined from the same method one would use in analysing a cantilevered beam subjected to a distributed load.

$$M = \int_{1.5}^{R} F_N r\, dr \tag{12}$$

$$\alpha_M = \frac{M\left(c_{root}\right)/2}{I_{root}} \tag{13}$$

The axial load on the root of the blade can also be found by simple determination of the component of the blade weight acting along the blade length for a given rotational position, combined with the centrifugal load from the radial motion.

$$F_{r1} = mr\Omega^2 \tag{14}$$

$$\mathrm{F}_{r2} = mg\sin\psi \tag{15}$$

$$F = F_{r1} - F_{r2} \tag{16}$$

$$\sigma_F = \frac{F}{A_{root}} \tag{17}$$

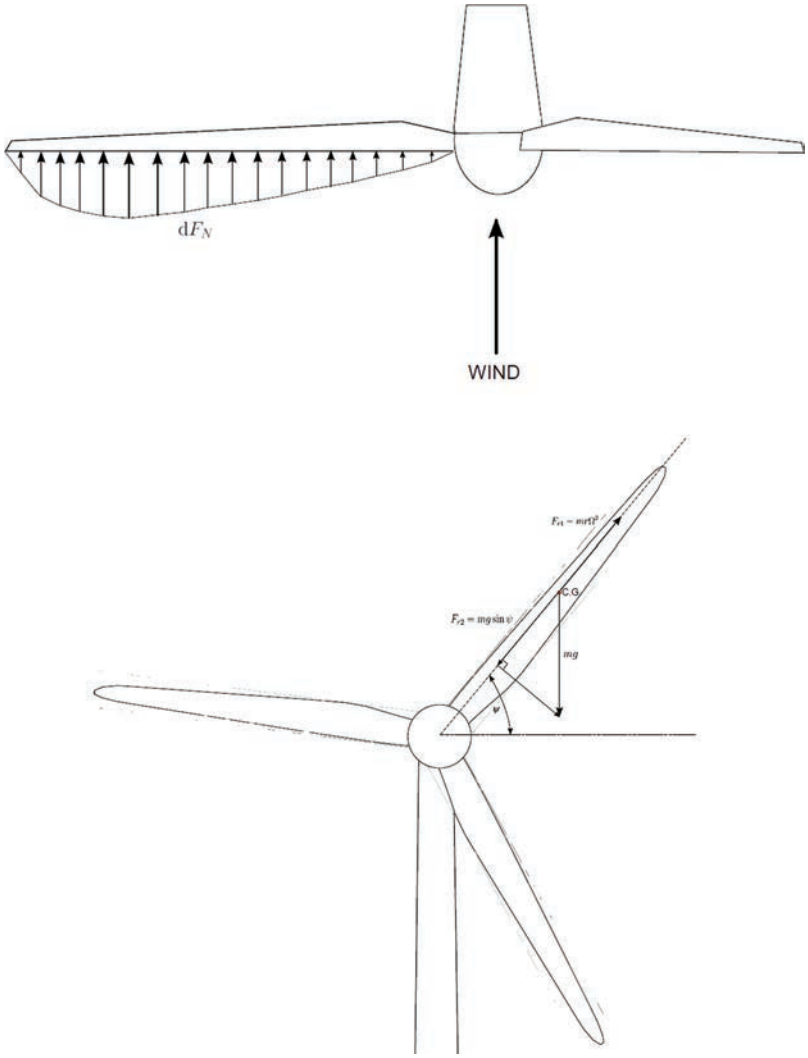

Figure 8. Diagram of the turbine loads being considered in the structural analysis of the blade

The combined flap-wise blade root stress is then given as:

$$\sigma = \sigma_M + \sigma_F \tag{18}$$

The typical flap-wise blade bending moment distribution is shown in Figure 9. The general flowchart of the computation is shown in Figure 10.

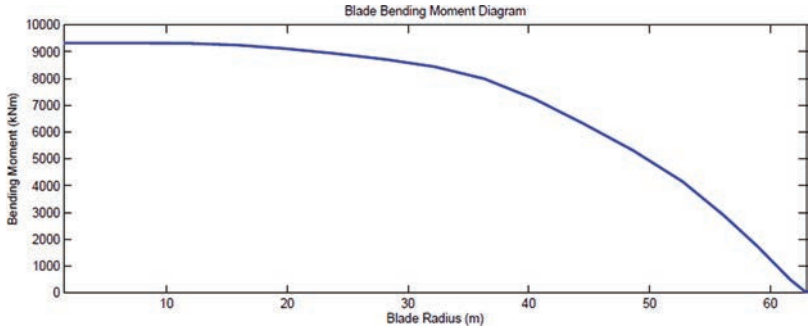

Figure 9. Flap-wise blade bending moment diagram

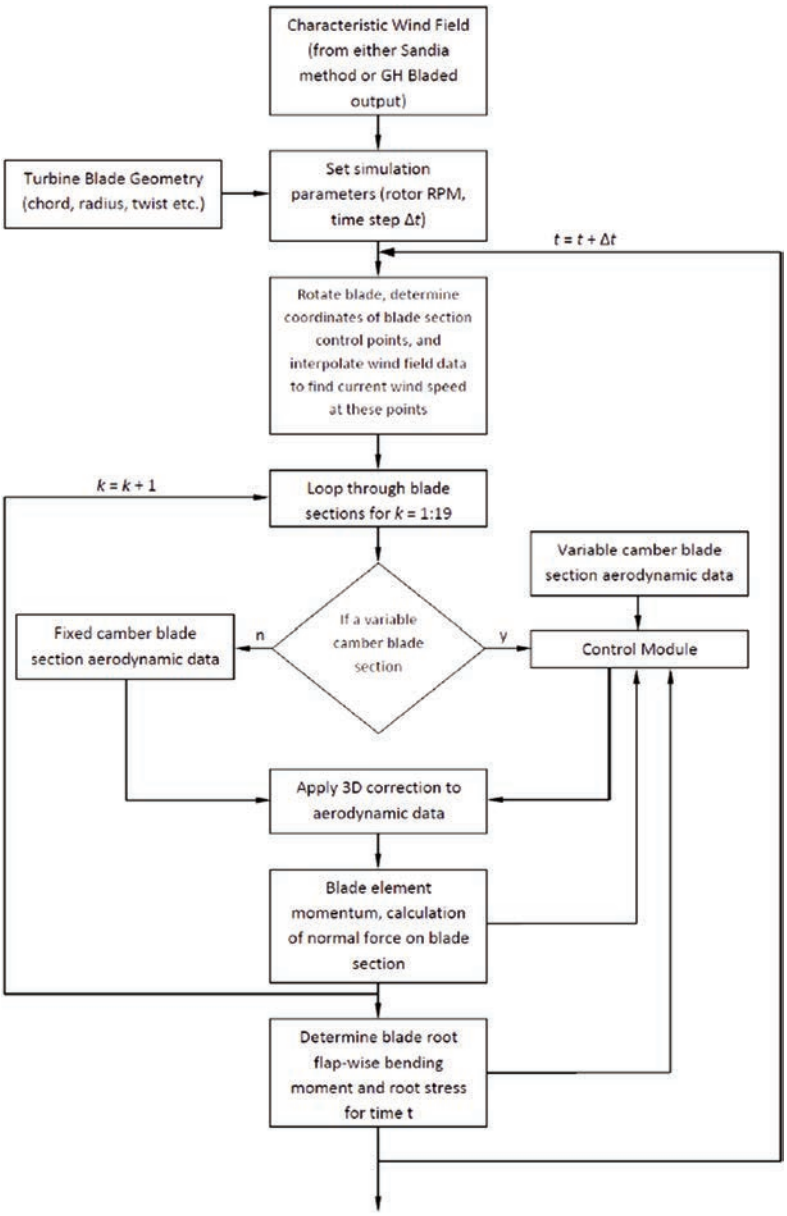

Figure 10. Graphical representation of the computational analysis routine

4. CONTROLLED LOAD ANALYSIS

4.1. Bending moment and root stress

The field of wind turbine active control system development is one that is very advanced. Control systems have been proposed and studied that employ complicated optimisation routines and advanced sensors, including the use of LIDAR to map the incoming wind field for use in feed-forward control. Replicating such advanced control is beyond the scope of this paper, yet investigation of the full load control potential of the preliminary design is desired. As such, a manual method is employed, whereby the optimum data points are selected from the plotted range of turbine control output, and resulting performance analysed. The result of the process is shown in Figure 11, whereby the resulting bending moment for maximum camber and minimum cambers on all control points (control points 13–19 in Table 1), and no control, are plotted. On top of this is plotted the optimum control outcome, a function which stays within the upper and lower bounds of performance whilst cutting out all high frequency disturbances, and limiting the range (standard deviation) of the maximum and minimum outputs. To reiterate, the optimal control output is

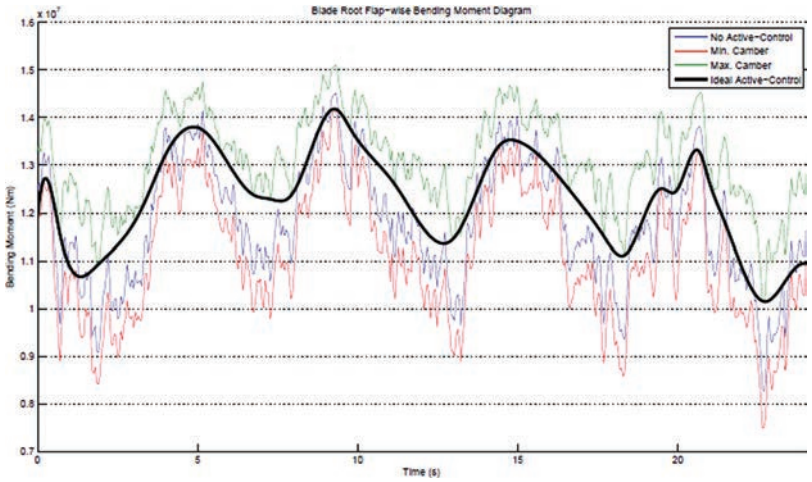

Figure 11. Resulting range of bending moment for different extremes of variable camber, allowing optimal control to be established

achieved by manually selecting points. These points alternate between lying on the maximum and minimum camber outputs. A spline is then generated from these points to show an optimally damped output. The result of the root stress is shown in Figure 12. A reduction in the standard deviation of the output in the order of 23% is observed with a slight increase of 4% in the mean value.

Barlas and van Kuik (2009) and Lackner and van Kuik (2011) work are the most appropriate piece of work to compare the above results to, as it is performed on the same wind turbine, and under similar wind conditions. In addition, the results are quantified in reduction in the standard deviation of the flap-wise, blade root bending moment, a value which unlike reduction in outright fatigue loading, is independent of measurement techniques, and easily quantified.

The equivalent result found in this work was a 16.35% reduction in flap-wise, blade root bending moment, which compares reasonably well to a reduction of 21.59% found for optimal control of the variable-camber blade despite of many differences in the modelling techniques between these two work. It seems fairly clear that the preliminary design developed in this report certainly has a similar performance range to TE flap devices investigated previously. As such, it is concluded that the design developed in this report develops meaningful load control, deemed beneficial, and necessary for the development of ever larger wind turbines into the future.

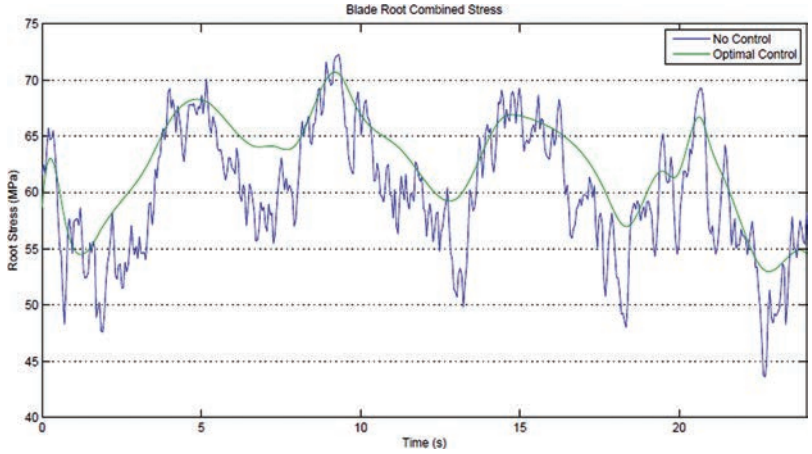

Figure 12. Resulting root stress (tension side) with optimal control, showing a 23% reduction in standards deviation and a 4.12% increase in the mean value over the no-control case

4.2. The importance of weight

The importance of weight in active load control is a topic that has received limited attention. This section outlines a brief investigation into the role blade weight plays in the effectiveness of active aerodynamic load control. As most evident from Figure 13, the bending stress, which is the result of aerodynamic forces alone accounts for upwards of 95% of the root stress. This leads to the result shown in Figure 13, whereby only a small change in the mean stress is observed when doubling the original blade mass of 40 tonnes. Of interest to active load control is the result in Figure 14, which shows the reduction in root stress standard deviation against the base weight case. Interestingly, an improvement is observed for the tension side, while a worsening of the control is seen in regards to the compression side. This highlights the complex interplay between the weight-related, cyclic stress component and the wind shear dominated bending stress. This sees the high bending stress coincide with the highest negative gravity load, whilst the lowest bending stress coincides with the highest positive gravity load, reducing the standard deviation of the tension stress observed. The opposite is true for the compressive side of the blade, where a 40% increase in blade weight reduces the effectiveness of the control by almost 30%. However, even an increase in blade weight of this order would still see a 13% reduction in the compressive root stress standard deviation, and meaningful load control.

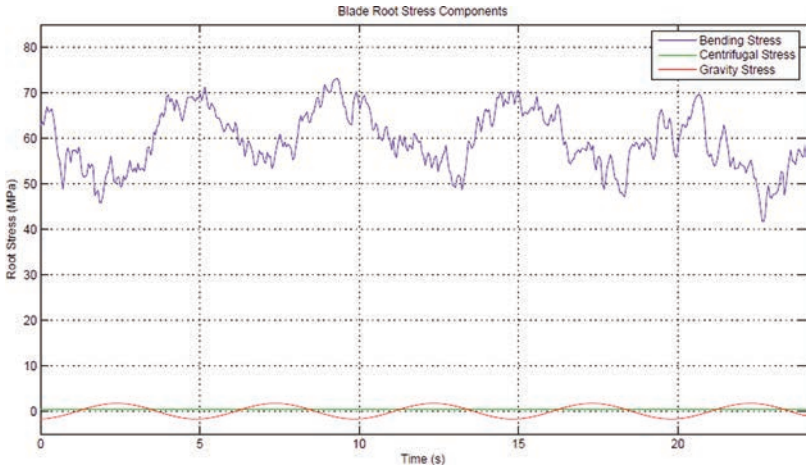

Figure 13. The three components of blade stress, with the weight-independent bending stress accounting for more than 95% of the loading

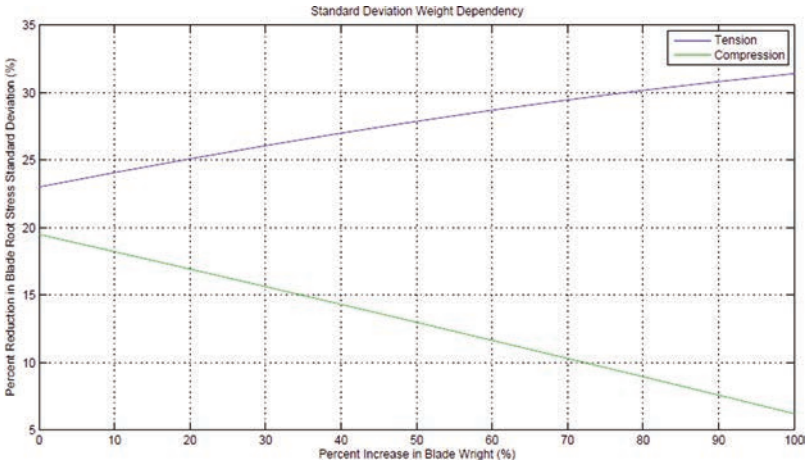

Figure 14. Plot showing the limited importance of weight to load control to blade root stress standard deviation, both to the tension and compression side of the blade root

5. CONCLUSIONS

This paper has scratched the surface of the true potential of wind turbine active aerodynamics. The work undertaken in this report has been a first step in moving from the proven theory of active aerodynamic load control to the reality of having active aerodynamic control employed on industrial-scale commercial wind turbines. Yet, it is hoped to make a valuable contribution to the field, in establishing a design that demonstrates a feasible path forward, for the application of active aerodynamics to real world turbine blades. The following are the main results of the analysis conducted in this report: (i) 21.59% reduction in the standard deviation of the blade root flap-wise bending moment was found possible with the variable-camber blade developed, (ii) the performance of the variable-camber blade was found to be comparable to that determined in similar studies of TE devices, and (iii) the proposed TE deformation mechanism design was deemed able to yield significant and meaningful load control.

REFERENCES

[1] Baker, D., Friswell, M.I., 2009. Determinate structures for wing camber control. Smart Materials and Structures 18, 035014.

[2] Barlas, T.K., van Kuik, A., 2009. Aeroelastic modeling and comparison of advanced active flap control concepts for load reduction on the upwind 5 MW wind turbine. The proceedings of the 2009 European Wind Energy conference & exhibition, 16–19 March 2009, Marseille, paper DT3B_3. (Available in: http://proceedings.ewea.org/ewec2009/proceedings/index.php?page=zip)

[3] Barlas, T.K., van Kuik, A., 2010. Review of the state of the art in smart rotor control research for wind turbines. Progress in Aerospace Sciences 46, 1–27.

[4] IEC 61400-1. Wind Turbines – part 1: Design Requirements. Geneva, Switzerland. Delrinhttp://www2.dupont.com/Plastics/en_US/Products/Delrin/Delrin.html

[5] Drela, M., 1989. XFOIL: An analysis and design system for low Reynolds number airfoils, Conference on low Reynolds number airfoil aerodynamics. University of Notredame. (Available in: http://web.mit.edu/drela/Public/papers/xfoil_sv.pdf)

[6] Gandhi, F., Frecker, M., Nissly, A., 2008. Design optimization of a controllable camber rotor airfoil, AIAA Journal 46, 142–153.

[7] Gupta, V., Sharma, M., Thakur, N., 2010. Optimization criteria for optimal placement of piezoelectric sensors and actuators on a smart structure: a technical review. Journal of Inteligent Material Systems and Structures 21, 1227–1243.

[8] Jensen, F., Andersen, B., Mangeot, C., Goueffon, C., 2007. New high performance piezoelectric actuator. Proceedings of SPIE - The International Society for Optical Engineering 6526, art. no. 65262X.

[9] Kota, S., Hetrick, J., Osborn, R., Paul, D., Pendleton, E., Flick, P., Tilmann, C., 2003. Design and application of compliant mechanisms for morphing aircraft structures. Smart Structures and Materials 2003: Industrial and Commercial Applications of Smart Structures Technologies, San Diego. (Available in http://www.flxsys.com/pdf/SPIE_2003_Paper.pdf)

[10] Lackner, M., Barlas, T., 2008. Smart rotor blade technology applied to the upwind reference turbine, The proceedings of the IEA topical expert meeting on the application of smart structures for large turbine blades, Sandia National Labs, Alberquerque, USA. (available in http://www.ieawind.org/Task_11/TopicalExpert/56_Smart%20Structures.pdf)

[11] Lackner, M. A., van Kuik, G.A.M., 2010 The performance of wind turbine smart rotor control approaches during extreme loads, Journal of Solar Energy Engineering, Trans. ASME, 132, 011008-1–011008-8.

[12] Lackner, M. A., van Kuik, G., 2011 A comparison of smart rotor control approaches using trailing edge flaps and individual pitch control, Wind Energy, 13, 117–134.

[13] Manwell, J.F., McGowan, J., Rogers, A., 2009. Wind energy explained: theory, design, and application. John Wiley, Hohoken, NJ.

[14] Marrant, B.A.H., van Holten, T.H., 2006. Comparison of smart rotor blade concepts for large offshore wind turbines, Offshore Wind Energy and other Renewable Energies in Mediterranean and European Seas OWEMES, European Seminar, Civitavecchia.

[15] Musial, W., Scott, G., Jonkman, J., Butterfield, S., 2009. Definition of a 5 MW reference wind turbine for offshore system development, Technical report NREL/TP-500-38060. (available in: http://mhk.pnnl.gov/wiki/images/b/bb/Jonkman_et_al_2009.pdf)

[16] Selig, M., Du, Z., 1998. A 3-D stall delay model for horizontal axis wind turbine performance prediction. AIAA, AA-98-0021.

[17] Veers, P.S., 1988. Three-dimensional wind simulation. Sandia Report, SAND88 – 0152 UC-261.

[18] Veers, P.S., Ashwill, T.D., Sutherland, H.J., Laird, D.L., Lobitz, D.W., Griffin, D.A., Mandell, J.F., Musial, W.D., Jackson, K., Zuteck, M., Miravete, A., Tsai, S.W., Richmond, J.L., 2003. Trends in the design, manufacture and evaluation of wind turbine blades. Wind Energy 6, 245–259.

[19] Winkelaar, D., 1992. Swift – program for three-dimensional wind simulation. ECN, ECN-R-92-013.